Supplementary Material

Toward Green Flotation: Interaction of a sophorolipid biosurfactant with a copper sulfide

[1]Priyanka Dhar, [1]Hakon Havskjold, [1]Maria Thornhill, [2,3]Sophie Roelants, [2,3]Wim Soetaert, [1] Hanumantha Rao Kota and [1]Irina Chernyshova**

[1]Department of Geoscience and Petroleum, Norwegian University of Science and Technology (NTNU), NO-7031 Trondheim, Norway
[2]Bio Base Europe Pilot Plant, Rodenhuizekaai 1, 9042 Ghent, Belgium
[3]Centre for Industrial Biotechnology and Biocatalysis (InBio.be), Department of Biotechnology (BW25), Faculty of Bioscience Engineering, Ghent University, Coupure Links 653, 9000 Ghent, Belgium

Table of Content

1. Biosynthesis and characterization of acidic sophorolipid (ASL)

ASL (1-carboxyl-dodecyl-β-D-glucopyranosyl-(1-2')-a-D-glucopyranose) was produced by the Bio Base Europe Pilot Plant, Ghent, Belgium, as described below.

1.1. Biosynthesis and purification

The production medium used for sophorolipids was described by Lang et al., (2001) and the strain used was the *S. bombicola* Δ*sble* strain described by Ciesielska *et al*.[1] selectively producing acidic sophorolipids.

Fed-batch fermentation was performed in a Biostat B culture vessel (Sartorius- BBI systems) with a maximum working volume of 1.5 L. Temperature, pH and pO_2setpoints were set at 30°C, 3.5 and 30 %respectively by the Biostat B control unit. In order to inoculate the bioreactor, 100 mL of an overnight grown shake flask culture (30°C, 200 rpm) was employed. The pH of the fermentation started at pH 5.8 and was allowed to drop spontaneously until pH 3.5 and 5 M NaOH was used to maintain this pH. Feeding of rapeseed oil was initiated 48 h after inoculation and was adjusted to the consumption rate. Additional glucose was added 150 h after inoculation. Sophorolipids were purified by applying a microfiltration step to remove the biomass, followed by a two-step ultrafiltration as described by Roelants et al.[2] Finally, hydrolysis of the mixture of acetylated and non-acetylated acidic SLs produced by this strain to obtain the acidic COOH form of SL is performed with 5 M NaOH solution followed by an ultrafiltration step to remove the salts.[2] The retentate of the last ultrafiltration step was then dried to an "off-white" powder by freeze drying.

Table S1. HPLC and GC analysis of ASL batch APS-DSP06

Parameter	%	Method
Dry Matter	98.72	Infrared balance 105°C
Glucose	0.015	HPLC-Metacarb
Glycerol	n.d.*	HPLC-Metacarb
Free fatty acid/alcohol content	<0.001	Internal method BBEPP GC with FID detector
Protein	< 1	BCA protein assay

*n.d. = below detection limit

1.2. Characterization of ASL

The purified product (batch # APS-DSP06) was analyzed using FTIR (**Figure S1**). The FTIR spectrum of ASL power was measured using a Bruker Vertex 80v spectrometer at a resolution of 4 cm^{-1} using a narrow band liquid nitrogen cooled MCT detector and a Platinum ATR accessory with a diamond ATR element. Its FTIR spectrum is similar to that reported by Baccile et al.[3] It shows that the carboxyl headgroup (the C=O peak occurs at 1720 cm^{-1}) is mostly in the protonated state.

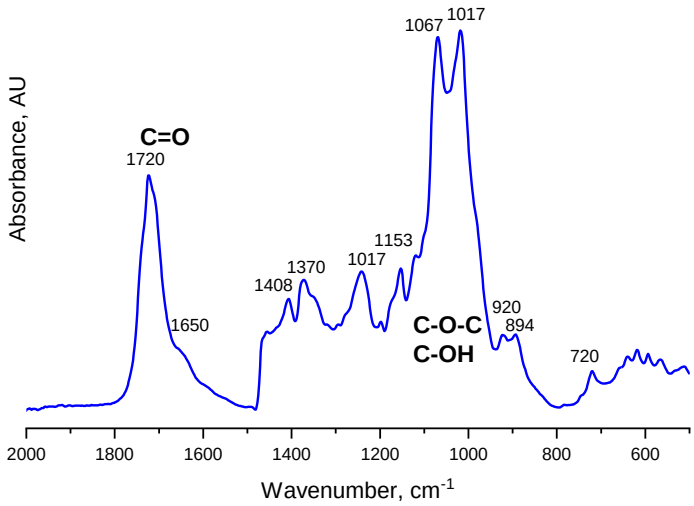

Figure S1. FTIR spectrum of ASL powder.

The residual glucose/glycerol and free fatty acids/oil (diethylether/heptane 50:50 extraction 1:1) were analyzed using high-performance liquid chromatography with an evaporative light scattering detector (HPLC-ELSD) and gas chromatography (GC) analysis with a flame ionization detector (FID), respectively[4] (**Table S1** and **Figure S2**). The final compound is primarily (>95%) comprised of acidic sophorolipids with 90.4% non-acetylated ASL C18:1 and 9.6% non-acetylated acidic sophorolipids with C18:0, C18:2 fatty acids.

Analysis of the ASL structure was done on micellar ASL solutions with ^{1}H and ^{13}C NMR ($CDCl_3/CH_3OD$=1:1). An average downfield shift from 172 ppm to 177 ppm was used as a reference to verify the formation of the COOH group. More info on the purification and characterization of ASL can be found in Ref.[2] ICP-MS revealed that the main metal impurity is Na, the concentration of which in 1 mM ASL solution is ca. 0.1 μM (**Table S3**). Multivalent metals are present in trace amounts.

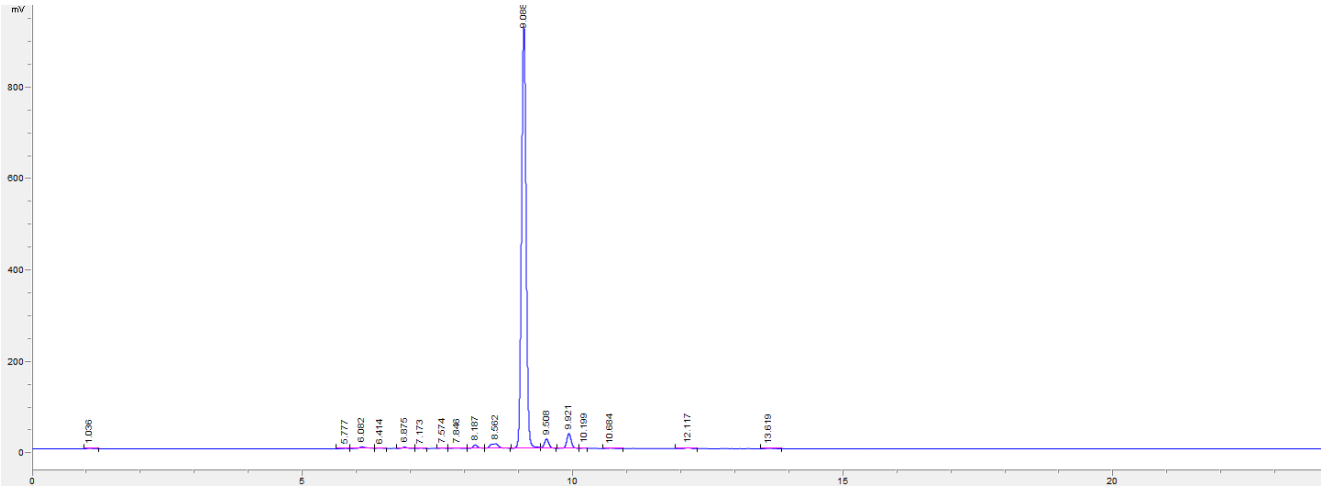

Figure S2. HPLC-ELSD chromatogram of ASL with the main peak being non-acetylated acidic SL C18:1 (**Scheme 1**).

Table S2. Composition based on peak areas in the HPLC-ELSD chromatogram of the ASL APS DSP06 product shown in **Figure S2**.

ASL component	Peak area	Amount (%)
Non-acetylated ASL C18:1 (main peak)	5426.6	90.4
Other sophorolipids (mainly non-acetylated ASL with incorporated C18:0, C18:2 fatty acids)	577.7	9.6

Table S3. ICP-MS analysis of a 1 mM (621.7 mg/L) ASL solution

Metal Ion	Concentration, µg/L	RSD, %
Na	2,103.6	1.9
Mg	2.46	4.0
Al	5.5	9.7
P	13.07	2.7
S	713	1.6
Ca	11.4	5.7
Ti	0.12	11.8
Fe	2.9	2.4
Cu	3.8	4.5

2. Characterization of Djurleite

Figure S3. Djurleite mineral as received from the supplier

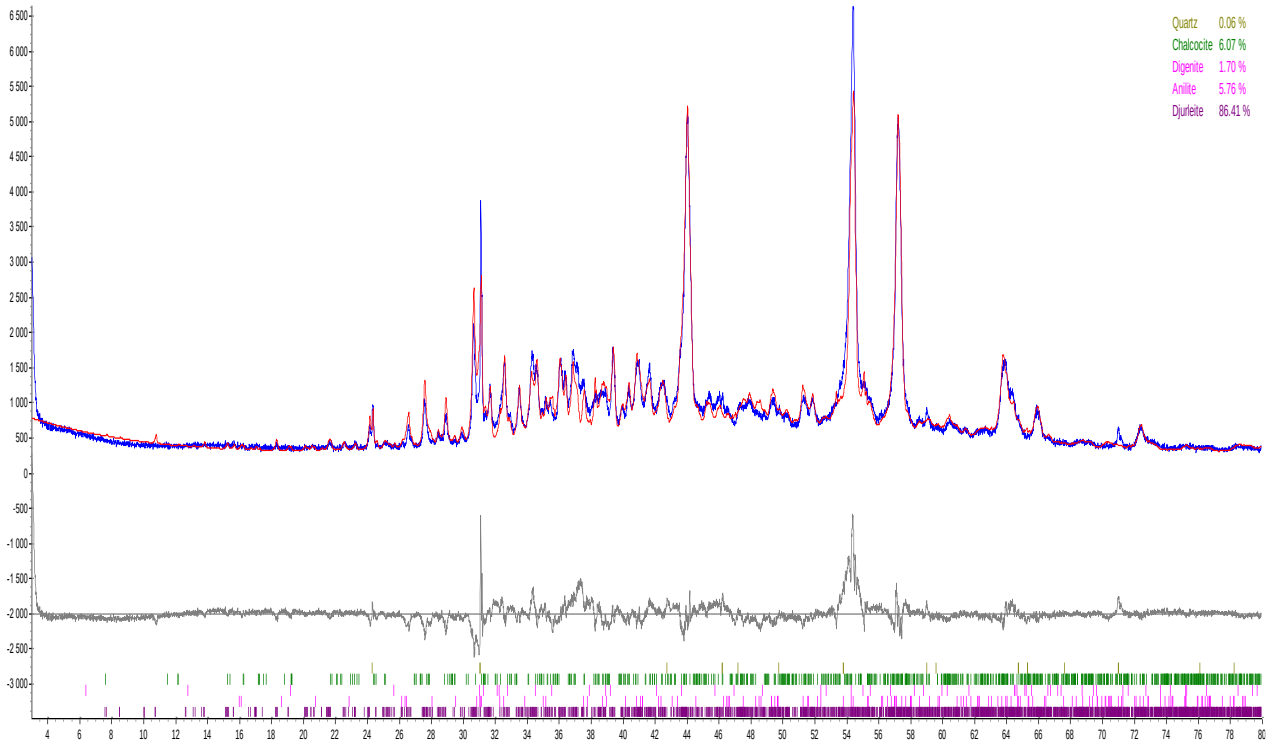

Figure S4. XRD of the –20 µm size fraction of djurleite

The phase composition of the minerals was analyzed by the X-ray diffraction (XRD) method using a BRUKER AXS D- advanced diffractometer with a *Co anode* (λ=1.79 Å). The detector used was LynxEye at 35 kV and a current of 40 mA. Scans were made in a 2θ range of 3–80° with a total exposure time of 70 min. For both the mineral powders a step size of 0.0116° was used.

XRD analysis (**Figure S4**) shows that the djurleite mineral consists of 86.4% of djurleite ($Cu_{1.94}S$), while the rest is other copper sulfides including 6.1% of djurleite (Cu_2S), 5.8 % anilite (Cu_7S_4), and 1.7% of digenite (Cu_9S_5).

3. Additional data

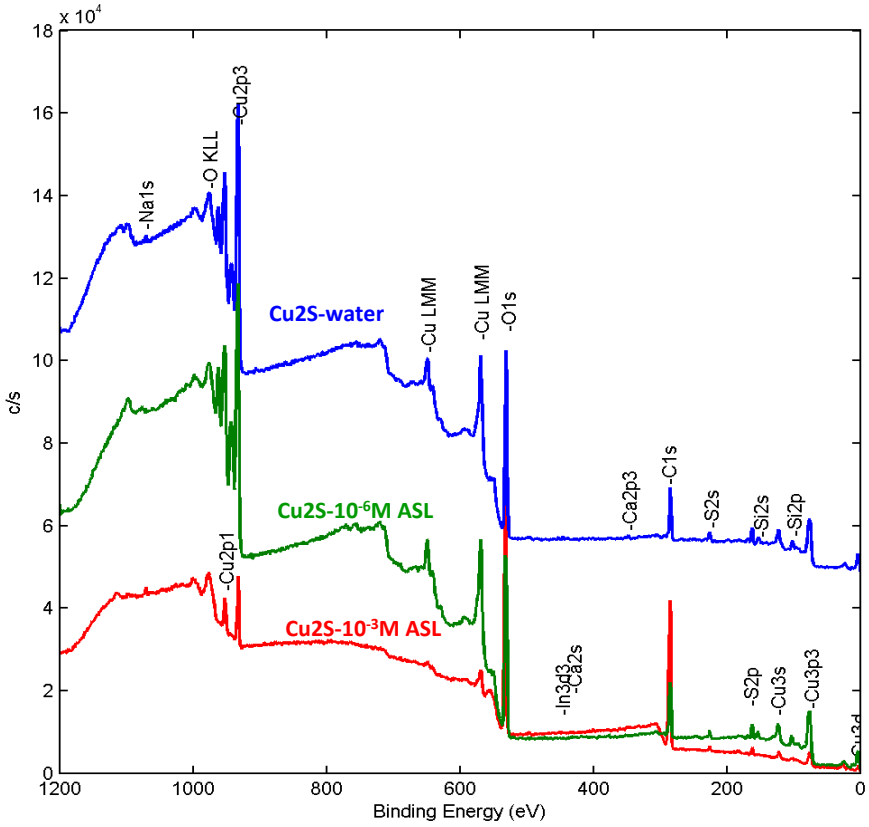

Figure S5. XPS survey spectra of djurleite particles conditioned in water, as well as in 10^{-6} and 10^{-3} M ASL solutions for 30 min. The conditioned particles were dried and mounted on an indium foil (**Figure S8**). The spectra show no In peaks. The most intensive peaks (In 3d) are expected at ca. 450 eV.

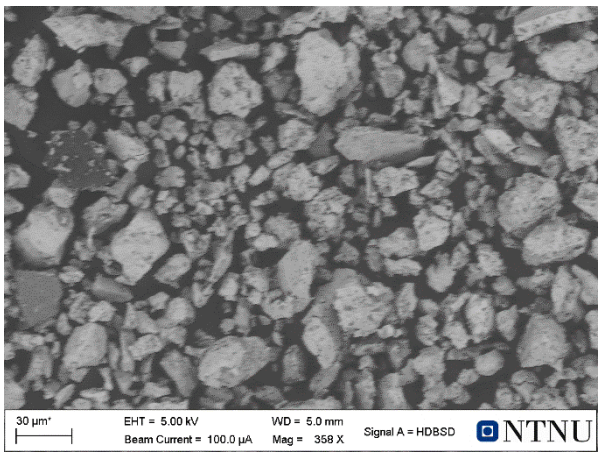

Figure S6. SEM of –20µm fraction conditioned in water at pH 7 for 30 min. The particles were adhered to a carbon tape. The image was obtained using a Zeiss EVO 50 scanning electron microscope at an electron high tension voltage of 5 kV.

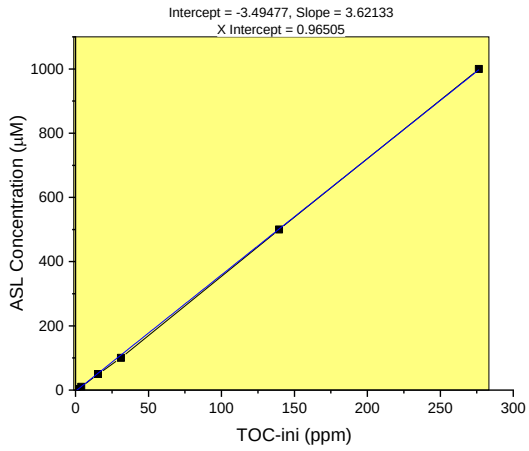

Figure S7. Calibration curve for the TOC analysis.

Figure S8. Mounting of sulfide particles on the XPS holder using an indium foil and double-sided carbon tape.

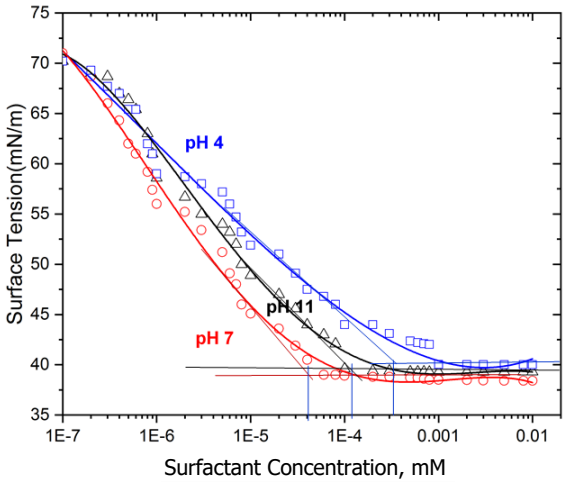

Figure S9. Extraction of the CMC values of ASL from surface tension

The surface tension (γ) values were used to determine the surface excess (Γ_{max}) and minimum surface area (A_{min}) of ASL at the air-water interface from the slope of the linear part of γ vs ln C using the following equations,[5-6]

$$\Gamma_{max} = -\frac{1}{nRT} \times \frac{d\gamma}{dlnC},$$

$$A_{min}=\frac{1}{N\Gamma_{max}},$$

where *R* is the gas constant (8.314 $J \cdot K^{-1} \cdot mol^{-1}$), *N* is the Avogadro's number, and *n* is the molecule specific dissociation number (the Gibbs prefactor). This number was taken as 1 at pH 4 and 7 on the basis of the earlier finding that ASL is weakly ionized at natural pH.[7] At pH 11, *n* was taken as 2 taking into account the pH dependence of the surface tension (Figure 1b) which suggests that most of the carboxyl groups of ASL are deprotonated at this pH.

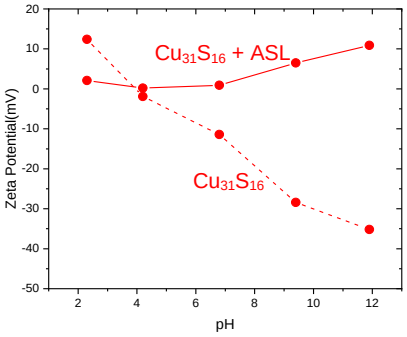

Figure S10. Effect of pH on zeta potential of –10 µm djurleite in water in the absence (dashed line) and presence (solid line) of $1x10^{-5}$ M ASL established in 5 min. The maximum standard deviation in triplicate measurement is 5 mV.

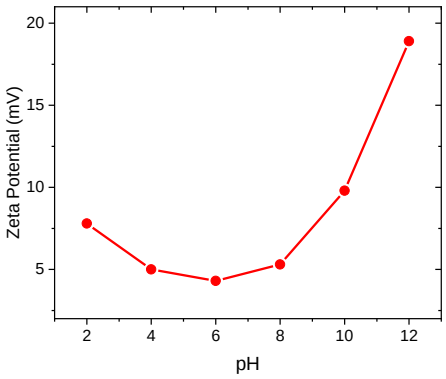

Figure S11. Zeta Potential of the ASL-Cu(II)-SO_4^{2-} precipitate as a function of pH in water. The maximum standard deviation in triplicate measurement is 5 mV.

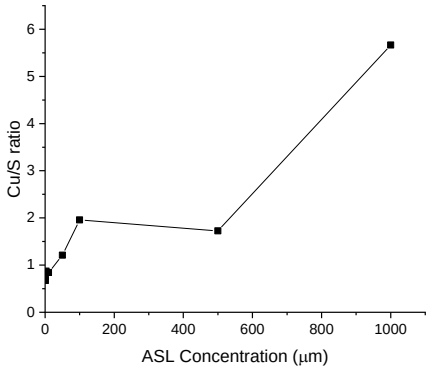

Figure S12. Effect of ASL concentration on the Cu/S ratio in solution from **Figure 3b**. The graph shows that dissolution of S and leaching of Cu dominates at low and high ASL concentrations, respectively.

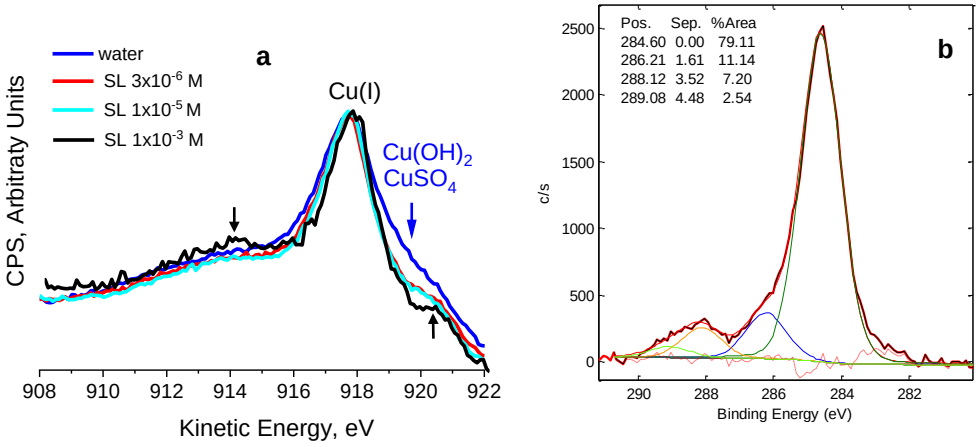

Figure S13. (**a**) Effect of ASL concentration on the Cu $L_3M_{4,5}M_{4,5}$ Auger peak of djurleite at pH 7 (corresponds to the XPS spectra shown in **Figure 9a** of the main text). (**b**) XPS C 1 spectrum of adventitious carbon on djurleite conditioned in water at pH 7. Black arrows in (a) show small peaks at 914 eV and 920.5 eV typical of Cu_2S. Interpretation is based on Refs.[8-9] The C 1s spectrum in (a) displays the principal peaks at 284.6 and 286.2 eV of the sp^3 saturated carbon and the carbon atoms bonded to oxygen, respectively.[10] Small peaks at 288.1 and 291.1 eV are in the range of carboxylate and carbonate groups, respectively.[10]

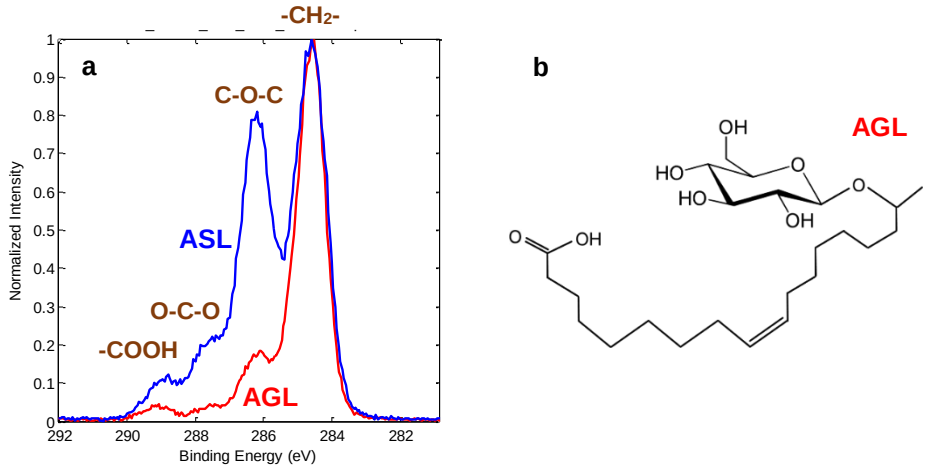

Figure S14. (**a**) Comparison of XPS C 1 s peaks of ASL and acidic glucolipid (AGL). (**b**) Chemical structure of AGL.

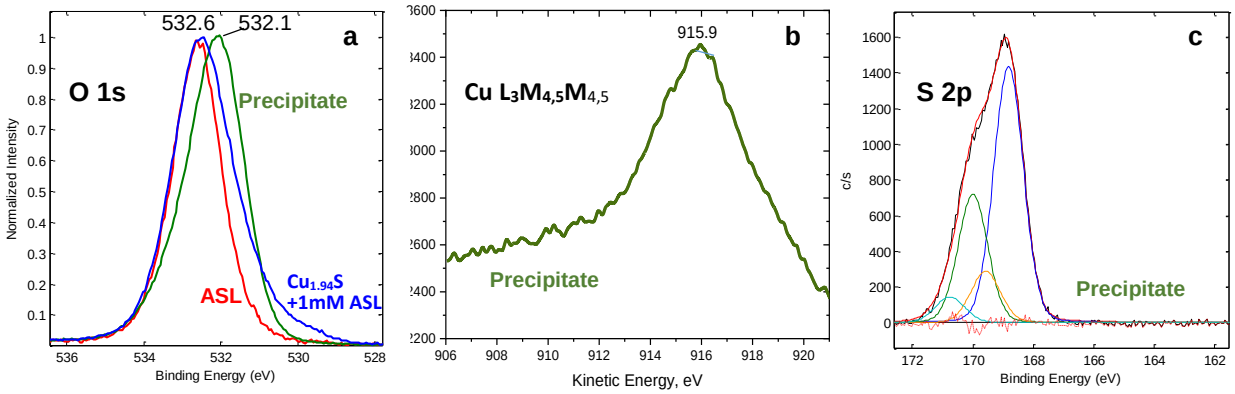

Figure S15. (a) Cu $L_3M_{4,5}M_{4,5}$ Auger, (b) XPS O 1s, and (c) S 2p spectra of the ASL-Cu(II)-SO_4^{2-} precipitate. (b) also shows for comparison the O1s peaks of solid ASL and djurleite conditioned at 1 mM ASL (pH 7). The S 2p spectrum in (c) is curve-fitted with two spin-orbit doublets, the main being at 168.8 eV, where the S 2p peak of Cu(II)SO_4 has been reported.[11]

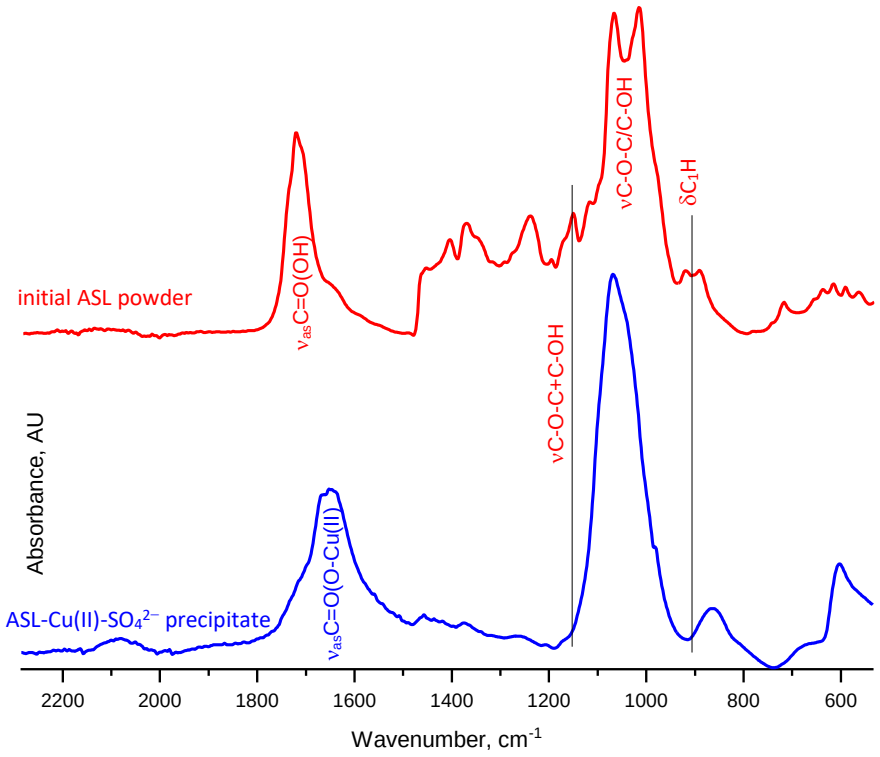

Figure S16. Comparison of ATR FTIR spectra of the ASL-Cu(II)-SO_4^{2-} precipitate and molecular ASL (initial surfactant in the powder form). The peak assignment can be found in Ref.[3]

To get complementary information about the coordination of the ASL headgroups in the ASL-Cu(II)-SO_4^{2-} precipitate, we compare its ATR FTIR spectrum with that of bulk ASL (**Figure S16**).

As seen from **Figure S16**, the sharp bands observed for the ASL powder become smeared in the case of the ASL-Cu(II)-SO_4^{2-} precipitate, which indicates that the latter is in the amorphous state. Importantly, the pronounced ν_{as}C=O(OH) peak at 1720-1700 cm^{-1} of the COOH group of ASL (which is mostly due to the C=O stretching) is replaced by a new structured band at 1650 cm^{-1}. This band is assigned to the asymmetric stretching vibration $\nu_{as}CO_2^-$ of the carboxylate group of a monodentate COO-Cu(II) complex. In fact, solid Na laurate is characterized by the $\nu_{as}CO_2^-$ band at 1560 cm^{-1}, while the Cu(II)-carboxylate chelating (bidentate mononuclear) complexes of fatty acids are characterized by the $\nu_{as}CO_2^-$ peak at ca. 1590 cm^{-1}.[12-13] The higher frequency of this vibration in the ASL-Cu(II)-SO_4^{2-} precipitate suggests that only one of the O atoms of its carboxylate groups is involved into the complexation with Cu(II). This finding supports the proposed formation of the ASL-Cu(II) ring complex (3).

In addition, **Figure S16** demonstrates that the sophorose bands of the precipitate at 800-1200 cm^{-1} are significantly different as compared to ASL. Specifically, a doublet at 1050 cm^{-1} is smeared out, which is ptoblematic to interpret as it is expected to have a contribution from the ν_{as}S-O stretching vibrations of coordinated SO_4^{2-}. However, the other changes strongly suggest that the sophorose group directly interacts with Cu(II). In particular, a peak at 1160 cm^{-1} assigned to the C–O–C glucosidic linkage stretch

coupled with C–OH stretch and OH deformation[3] disappears. In addition, a band due to the axial C_1H deformation doublet at 900 cm^{-1} transforms to a broad singlet shifted to 860 cm^{-1}.

Hence, the FTIR spectra fully corroborate the XPS-based conclusion that both the headgroups of ASL are coordinated by Cu(II) in the precipitate, as well as support the formation of the ASL-Cu(II) ring complex (3).

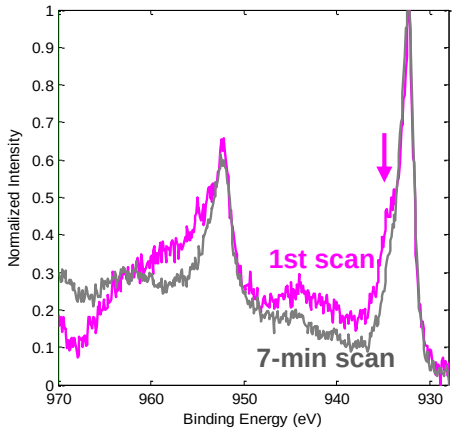

Figure S17. Effect of the exposure to the XPS conditions on the Cu 2p spectrum of djurleite conditioned in a 10^{-3} M ASL solution at pH 7. The first scan demonstrates a higher relative intensity of the Cu(II) component (labelled by an arrow).

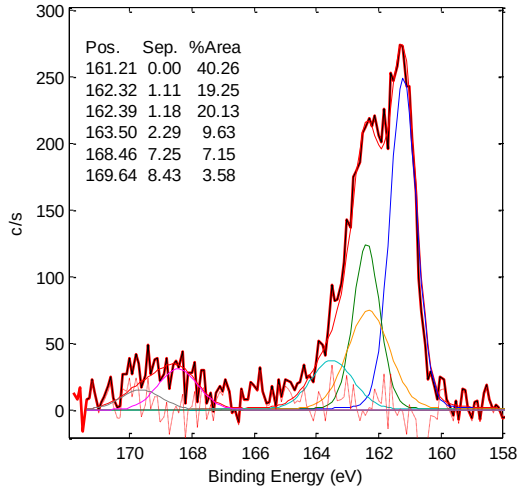

Figure S18. Curve-fitted XPS S 2p spectrum of djurleite conditioned in 1-mM ASL solution at pH 7 (**Figure 9c**). It shows three duplets with the main peaks at 161.2, 162.3, and 168.5 eV assigned to the S atoms of djurleite, polysulfides, and sulfate, respectively.

References

1. Ciesielska, K.; Roelants, S. L. K. W.; Van Bogaert, I. N. A.; De Waele, S.; Vandenberghe, I.; Groeneboer, S.; Soetaert, W.; Devreese, B., Characterization of a novel enzyme—Starmerella bombicola lactone esterase (SBLE)—responsible for sophorolipid lactonization. *Appl. Microbiol. Biotechnol.* **2016,** *100* (22), 9529-9541.
2. Roelants, S. L. K. W.; Ciesielska, K.; De Maeseneire, S. L.; Moens, H.; Everaert, B.; Verweire, S.; Denon, Q.; Vanlerberghe, B.; Van Bogaert, I. N. A.; Van der Meeren, P.; Devreese, B.; Soetaert, W., Towards the industrialization of new biosurfactants: Biotechnological opportunities for the lactone esterase gene from Starmerella bombicola. *Biotechnol. Bioeng.* **2016,** *113* (3), 550-559.
3. Baccile, N.; Noiville, R.; Stievano, L.; Bogaert, I. V., Sophorolipids-functionalized iron oxide nanoparticles. *PCCP* **2013,** *15* (5), 1606-1620.
4. Van Renterghem, L.; Roelants, S. L. K. W.; Baccile, N.; Uyttersprot, K.; Taelman, M. C.; Everaert, B.; Mincke, S.; Ledegen, S.; Debrouwer, S.; Scholtens, K.; Stevens, C.; Soetaert, W., From lab to market: An integrated bioprocess design approach for new-to-nature biosurfactants produced by Starmerella bombicola. *Biotechnol. Bioeng.* **2018,** *115* (5), 1195-1206.
5. Pugh, R.; Stenius, P., Solution chemistry studies and flotation behaviour of apatite, calcite and fluorite minerals with sodium oleate collector. *Int. J. Miner. Process.* **1985,** *15* (3), 193-218.
6. Fainerman, V. B.; Möbius, D.; Miller, R., *Surfactants: Chemistry, Interfacial Properties, Applications*. 1st ed.; Elsevier: New York, Amsterdam, 2001; Vol. 13.
7. Penfold, J.; Thomas, R. K.; Shen, H. H., Adsorption and self-assembly of biosurfactants studied by neutron reflectivity and small angle neutron scattering: glycolipids, lipopeptides and proteins. *Soft Matter* **2012,** *8* (3), 578-591.
8. Velasquez, P.; Leinen, D.; Pascual, J.; Ramos-Barrado, J. R.; Cordova, R.; Gomez, H.; Schrebler, R., XPS, SEM, EDX and EIS study of an electrochemically modified electrode surface of natural chalcocite (Cu2S). *J. Electroanal. Chem.* **2001,** *510* (1-2), 20-28.
9. Biesinger, M. C., Advanced analysis of copper X-ray photoelectron spectra. *Surf. Interface Anal.* **2017,** *49* (13), 1325-1334.
10. Beamson, G.; D. Briggs, D., *High Resolution XPS of Organic Polymers – The Scienta ESCA300 Database*. Wiley: New York, NY, 1992; p 295.
11. Vasquez, R. P., CuSO4 by XPS. *Surf. Sci. Spectra* **1998,** *5* (4), 279-284.
12. Robertson, E. J.; Beaman, D. K.; Richmond, G. L., Designated Drivers: The Differing Roles of Divalent Metal Ions in Surfactant Adsorption at the Oil–Water Interface. *Langmuir* **2013,** *29* (50), 15511-15520.
13. Otero, V.; Sanches, D.; Montagner, C.; Vilarigues, M.; Carlyle, L.; Lopes, J. A.; Melo, M. J., Characterisation of metal carboxylates by Raman and infrared spectroscopy in works of art. *Journal of Raman Spectroscopy* **2014,** *45* (11-12), 1197-1206.